Nuclear Engineering and Technology xxx (xxxx) xxx

Contents lists available at ScienceDirect

Nuclear Engineering and Technology

journal homepage: www.elsevier.com/locate/net

Original Article

Thermoluminescence characterization of biochar material for dosimetric applications

Umme Muslima [a], Mayeen Uddin Khandaker [a,b,c,*], S.N. Mat Nawi [a], S.E. Lam [a], S.F. Abdul Sani [d], D.A. Bradley [a,e], Mustafa Mahmoud [f], H.J. Woo [g]

[a] Applied Physics and Radiation Technologies Group, CCDCU, School of Engineering and Technology, Sunway University, Bandar, Sunway, 47500, Selangor, Malaysia
[b] Department of Physics, College of Science, Korea University, 145 Anam-ro, Seongbuk-gu, Seoul, 02841, Republic of Korea
[c] Faculty of Graduate Studies, Daffodil International University, Daffodil Smart City, Birulia, Savar, Dhaka, 1216, Bangladesh
[d] Department of Physics, Faculty of Science, Universiti Malaya, 50603, Kuala Lumpur, Malaysia
[e] School of Mathematics and Physics, University of Surrey, Guildford, GU2 7XH, United Kingdom
[f] Department of Radiological Sciences, College of Applied Medical Sciences, King Khalid University, Abha, 61421, Saudi Arabia
[g] Centre for Ionics, Universiti Malaya, Department of Physics, Faculty of Science, 50603, Kuala Lumpur, Malaysia

ARTICLE INFO

Keywords:
Low-cost carbonaceous biochar
Cobalt-60 gamma irradiation
Thermoluminescence dosimeter
X-ray diffraction
Raman spectra analysis

ABSTRACT

The purpose of this work is to evaluate the appropriateness of biochar, a carbon-rich substance developed from biowaste, as a passive radiation dosimeter by examining its structural and thermoluminescence (TL) properties. Various parameters related to the TL dosimetry of commercially available and eco-friendly biochar were analyzed, including effective atomic number, reproducibility, TL glow curve, dose-response linearity, sensitivity, and fading. The acquired results demonstrate that the response of the tissue equivalent biochar is linear with greater sensitivity to gamma-ray doses ranging between 2 and 200 Gy, along with excellent repeatability within a 3 % standard deviation. Fading studies conducted in both light and dark environments revealed a TL signal loss of 17 % after 28 days in an ambient light environment and 19 % in a dark room condition. Confocal Raman spectroscopy was employed to analyze the vibrational spectra and structural changes induced by radiation. Structural alterations within the examined dose range were further validated by measuring crystallite size (Lc), dislocation density (δ), lattice strain (ε), and FWHM (full width at half maximum) from XRD (X-ray diffraction) patterns. Based on these findings, biochar demonstrates promising dosimetric properties and can be developed into a cost-effective radiation dosimeter for industrial and medical applications.

1. Introduction

Modern advancements in radiotherapy can be attributed to the increasing adoption of highly precise in-vivo dosimetry technologies possessing improved spatial resolution. This is because the goal of radiation treatment is to control the radiation dose to the target volume in both phantom and in vivo scenarios for both externally and internally supplied fields, while also reducing the radiation to the surrounding normal tissue [1,2].

Carbon-based dosimeters can offer a cost-effective radiation monitoring option than conventional dosimetry techniques, especially when considering their resilience, reusability, and ease of development. Researchers have examined carbon-rich materials for dosimetry applications; in particular, investigations have been carried out on the properties of thermoluminescence and associated structural alterations that follow radiation exposure at doses ranging from 0.2 to 100 Gy. Single-wall carbon nanotubes (SWCNT) and bucky paper [3–5], two grades of pencil lead (2B and 8H) [6] have been analyzed to observe the structural alterations in graphite-rich mixtures subjected to radiation exposure by using X-ray photoelectron spectroscopy (XPS) and Raman spectroscopy. It has also been suggested that commercial pencil leads made of graphitic material, with a thickness of 0.3 mm, offer remarkable value for dosimetry-related solutions [7,8] as it is available in low cost and low photon energy dependent, but their use has limitations due to their brittleness and inconsistent carbon content. Another carbon-rich material that has been studied and shown promising results for

* Corresponding author. Applied Physics and Radiation Technologies Group, CCDCU, School of Engineering and Technology, Sunway University, 47500, Bandar Sunway, Selangor, Malaysia.
E-mail addresses: mu_khandaker@yahoo.com, mayeenk@sunway.edu.my (M.U. Khandaker).

https://doi.org/10.1016/j.net.2024.103348
Received 14 July 2024; Received in revised form 24 October 2024; Accepted 28 November 2024

tracking the radiation dosage within the human body is graphite sheets [9]. It has a great deal of potential to fulfill thermoluminescence dosimetry (TLD) criteria for medical applications, although because of its density, certain modifications are necessary.

Since carbonaceous material demonstrated very encouraging findings in those studies, it may serve as the basis for the development of a next-generation thermoluminescence (TL) dosimeter for medical applications. The paucity of research in this field has highlighted a knowledge gap and motivated the development of an affordable carbon-based thermoluminescence dosimeter as a radiation dosimetry solution.

Biochar can be a low-cost dosimetry solution, made from waste material and has unique chemical and physical properties like high porosity and hydrophobicity. It is produced through pyrolysis at a temperature below 700 °C without the presence of oxygen. The structure of biochar contains a variety of pores, including macro, meso and micropores. The fact that these pores can interact with other substances to produce structural defects, which is a helpful feature in dosimetry [10,11]. The pores can also increase the surface area. The hydrophobicity of biochar, in particular, prevents it from readily interacting with water molecules, addressing the hygroscopic issue found in some commercial dosimeters, such as lithium fluoride (LiF)-based thermoluminescent dosimeters. This property helps to maintain the stability and accuracy of the dosimeter's readings under varying humidity conditions. Yan et al. [12] investigated the structure of biochar by XRD and confirmed that pyrolysis temperature plays a crucial role in the structure of biochar. This study also investigated the chemical structure of biochar by raman spectroscopy and reported on defects in biochar. Sahoo et al. [13] also performed the structural and morphological analysis of biochar from the different substances (e.g. bamboo, pegion pea stalk) and reported the effect of pyrolysis temperature on the structure with the elemental composition of each type. Although these investigations validate the distinct chemical and physical characteristics that can be employed to emphasize possible applications as a dosimeter, they are still unexplored.

This work aims to explore the TL dosimetric properties (such as linearity, sensitivity, repeatability, TL glow curves, linearity index, and fading) of biochar exposed to ^{60}Co gamma radiation within the dose range of 2–200 Gy. SEM/EDX analysis has been performed to observe the elemental composition and calculation of the effective atomic number (Z_{eff}) of the studied material. Furthermore, the structural analysis has also been performed using X-ray diffraction (XRD) and Raman spectroscopy, a dosimetrically useful technique [14]. The structural changes brought on by the radiation doses will also be observed using XRD and Raman spectra within the dose ranges 2–200 Gy. Specifically, the research interest is in investigating the possible use of biochar as an affordable, effective passive radiation detector that offers high spatial resolution and tissue equivalency.

2. Experiment and methods

2.1. Collection and preparation of sample

In this study, coconut shell biochar was purchased from a commercial supplier, Shopee, Malaysia. The biochar was produced through a pyrolysis process carried out in the absence of oxygen at temperatures below 700 °C. The collected samples were ground and crushed into a fine powder using a mortar and pestle. The powdered biochar was then sieved with a micrometer mechanical sieve (Thermo Fisher Scientific) to obtain a uniform grain size of 250 μm. For the experiments, samples weighing 10–15 mg were selected to fit within the TLD reader's 5 × 5 mm^2 planchet.

2.2. Annealing of sample and storage process

The TL intensity of the carbonate matrix is influenced by a variety of defects [15,16]. For this reason, the samples underwent annealing to eliminate any pre-irradiation memory, such as triboluminescence, and to obtain the accurate TL intensity by lowering the background noise signals. A programmable furnace (CMTS model MB 3) installed at the University of Malaya, Malaysia, was used to anneal the samples, which entailed heating them to an optimized heating temperature of 400 °C for an hour [17]. To prevent contamination and sample loss during the annealing process, the samples were placed into the multi-user furnace using a ceramic container and then covered with aluminum foil. Following the annealing procedure, the specimens were allowed to reach ambient temperatures slowly. The changes in cooling rate have been demonstrated to have an impact on the measured trapping parameters and TL sensitivity in a variety of luminous materials [18].

2.3. Irradiation of sample

Irradiation for gamma was made using a^{60}Co Gammacell-220 facility (mean energy 1.25 MeV) at the Department of Physics, University of Malaya, with a dose rate of 0.070 Gy/s at the time of investigation on the samples. The studied biochar was exposed to a dose range of 2–200 Gy The samples were positioned at the center of the chamber to ensure a homogeneous dose distribution at room temperature. The experimental and irradiation setups are shown in Fig. S1.

2.4. Characterization

2.4.1. Sample readout

The irradiated samples were read out 24 h after the irradiation employing a Harshaw 3500 TL reader (USA) equipped with WinREMS support software. This reader contains a sample drawer that can accommodate a single-element TL dosimeter, a programmable linear heating system, and a cooled photomultiplier tube that has the essential electronics to measure the amount of TL light output. TL intensity was assessed in a slow flow of N_2 gas atmosphere in order to mitigate triboluminescence and oxidation issues. In this work, the reader's Time-Temperature Profile (TTP) characteristics were configured by adjusting the preheat temperature to 50 °C and acquiring data at a temperature ramp rate of 10 °C/s up to a maximum of 300 °C for 25 s. The maximum temperature for acquiring data was optimized for biochar. The background radiation was subtracted automatically within the software as it was reading the sample.

2.4.2. Elemental analyses by SEM/EDX

Scanning electron microscopy/energy dispersive X-ray spectroscopy (SEM/EDX) is a useful technique for figuring out the mass influences of each element in a material. The name and ratio of each contributing element in the materials under examination are useful to know whether the material is appropriate to be utilized as a TL dosimeter. This allows for the calculation of the effective atomic number. Magnified cross-sectional pictures were taken using a TESCAN VEGA3 SEM apparatus equipped with the Oxford Instruments EDX system, which is situated at Sunway University. The elemental composition of the biochar was then examined.

2.4.3. Structural analysis of biochar

2.4.3.1. Raman spectra analysis. Utilizing Raman spectroscopy, defects in the material under study were evaluated. The structure of biochar was investigated using WITec alpha300 RA confocal Raman spectroscopy in this work. The samples were stimulated using a green laser light (532 nm; energy 2.33 eV) and a 50 × objective lens. The scattered Raman signal was detected using an optical grating of 300 g mm^{-1}. It was then transmitted via an optic multifibre to a spectrometer, where it was recorded for 10 s. To observe the radiation-induced defect, the peak of the D band and G band will be examined for biochar samples with ^{60}Co gamma exposure within the dose range of 2 Gy–200 Gy.

2.4.3.2. X-ray diffraction (XRD) analysis. An XRD diffractometer (Malvern PANalytical system model Empyrean) fitted with a standard Cu–Kα radiator and set to operate at 40 kV and 40 mA was used to analyze the structure of the biochar samples. A copper target of the radiator is used to generate Cu Kα1 8.04 keV X-ray at room temperature. Using the Bragg-Brentano geometry diffraction method, XRD measurements were made for 2 theta values ranging from 5 to 80 at a scanning step time of 148.92 s and a step size of 0.0260°. The Bragg equation (1) was used to find the value of the atomic spacing, or d (the prominent line), and the Scherrer equation (2) was employed to estimate the crystallite size parallel to the c-direction, or L_c [19]. From the XRD pattern of biochar, the lattice parameter, unit cell volume, lattice strain and dislocation density were examined. The following equations are as follows:

$$\text{Atomic spacing, } d = \frac{\lambda}{2\sin\theta} \tag{1}$$

$$\text{Crystallite size, } L_c = \frac{k\lambda}{\beta\cos\theta} \tag{2}$$

where λ is the wavelength of X-ray radiation (λ = 0.154 nm), θ is the Bragg angle (angle between incident rays and the crystal surface) in radians, β is the full width at half maximum (FWHM) in radians and k is Scherrer's constant (k = 0.94).

$$\textit{Volume of the unit cell}, V = abc\sqrt{1-\cos^2\alpha-\cos^2\beta-\cos^2\gamma-2\cos\alpha\cos\beta\cos\gamma} \tag{3}$$

$$\textit{Dislocation density}, \delta = \frac{1}{L_c{}^2} \tag{4}$$

Where, L_c is the crystallite size.

$$\textit{Lattice strain}, \epsilon = \frac{\beta}{4\tan\theta} \tag{5}$$

3. Results

3.1. Elemental analysis and effective atomic number for biochar

Knowledge of the effective atomic number (Z_{eff}) of an absorbing material is crucial for evaluating the thermoluminescence (TL) properties of a composite material containing that absorber. The Z_{eff} of the biochar was determined using the well-known Mayneord equation Eq. (6a) [20].

$$Z_{eff} = \left(a_1 z_1^m + a_2 z_2^m + a_3 z_3^m + \ldots\ldots a_n z_n^m\right)^{1/m} \ldots\ldots\ldots\ldots \tag{6a}$$

The fractional weights of each element in the dosimeter are represented by the values a_1, a_2, a_3, … a_n. In practical terms, the power dependency of m of 2.94 is thought to be the best fit when accounting for the photoelectric dominant interaction. Eq. (6b) was used to calculate the number of electrons per gram (N_e) of samples, as follows:

$$N_e = \frac{N_A Z}{A_w}(W) \quad \ldots\ldots\ldots\ldots \tag{6b}$$

Where, N_A is the Avogadro number, Z is the atomic number of each element, A_w is the atomic weight, W is the fractional weight of an element.

To determine the elemental contributions of elements like carbon, oxygen, potassium, and calcium, SEM–EDX analysis was performed (see Table 1). Table 1 presents the elemental composition data as well as the effective atomic number (Z_{eff}) for the samples. Fig. S2 demonstrates the SEM image to see the morphological structure of biochar. For the elemental distribution analysis of biochar, we utilized the point technique, conducting measurements at a total of 2 spots for 4 aliquots to obtain the mean average distribution of each element in biochar. This approach ensures a representative analysis of the elemental composition across multiple samples. The Z_{eff} value of 7.05 is found for biochar, which is very close to the Z_{eff} value of human soft tissue. It is advantageous for a dosimeter in clinical dosimetry to have soft tissue equivalent (Z_{eff} = 7.46) in order to assure response independence based on incident photon energy.

Table 1
Elemental composition from EDX analysis and Effective atomic number for biochar.

Elements	Elemental compositions for Biochar sample	
	Weight (%)	Atomic (%)
C	94.22	96.50
K	1.63	0.51
Ca	0.45	0.14
O	3.70	2.85
Z_{eff}	7.05 ± 0.01	

3.2. Structural analysis by Raman spectroscopy

Raman spectroscopy is a powerful, non-invasive method that may be used to inspect the carbonaceous crystalline lattice for flaws and faults [21–23]. It is also quite sensitive when analyzing carbon allotropes [24,25]. A wide range of information, including doping, thickness, disorder, grain and edge boundaries, strain, and thermal conductivity, is available under various physical situations [26]. Table S1 provides more details on the formation of disorder/defect modes in the carbon media used in this investigation. Here, five unique peaks-referred to as D, G, D′, G′(2D), and (D + G) bands, are shown in the analysis of the biochar Raman spectra. These peaks are located at approximately 1347, 1585, 1954, 2315, and 2945 cm^{-1} respectively (Fig. S3(a)). The G band at 1585 cm^{-1} is produced by the in-plane stretching of the hexagonal carbon rings or the stretching vibration of sp^2 carbon (E_{2g} symmetry) [27]. The D peak, a defect mode located at around 1347 cm^{-1}, represents sp^3 electronic states. These states are connected with the vibration of carbon atoms in disordered graphite, which includes defects, dangling bonds in plane terminations, and grain boundaries. These states are thought to be defects in planar sp^2 graphitic structure. According to Ref. [12], the investigated sample's wave numbers for the D and G bands demonstrate that it is in agreement with biochar. Another double-resonance Raman characteristic of disorder and defects is the D′ bands [28]. The D′ peak, which appears at roughly 1954 cm^{-1}, is indicative of flawed graphite-like material and the 2D peak, at 2315 cm^{-1}, is thought to be an overtone of the D peak. Table S1 lists the specifics of the vibrational modes for biochar. From Fig. S3(a) it can be observed that the peak width of the D band is greater than the G band. The I_D/I_G ratio of 1.18 obtained from the D band and G band of non-irradiated studied biochar indicates that the investigated biochar was produced by low-temperature pyrolysis and has an appropriate degree of defects [12]. Functional groups from the coconut shell were not destroyed during pyrolysis [29]. This exploratory work also evaluated the use of micro-Raman spectroscopy to detect radiation damage in gamma-ray exposed biochar at different doses ranging from 0 to 160 Gy by analyzing defect states. Fig. S3(b) represents the raman spectra for biochar samples irradiated with doses 0–160 Gy. Table S2 gives the summary of dose-dependent change in the D band for ^{60}Co irradiated biochar. It can be observed that the intensity, area and FWHM of the D band are changing with the doses of gamma irradiation, indicating the structural alteration due to radiation-induced defects. The data indicates that the full-width half maxima (FWHM) of the D band shows variations with increasing doses, initially increasing at lower doses and then decreasing slightly at higher doses, suggesting changes in crystallinity and defect density. The intensity of the D band fluctuates across the dose range, with a notable increase at 200 Gy, indicating a rise in defect density and disorder within the biochar structure. Additionally, the area under the D band varies, reflecting the extent of radiation-induced

structural modifications, with significant increases at lower doses and a marked peak at 200 Gy, suggesting enhanced trapping sites for charge carriers. These findings confirm that gamma irradiation induces structural alterations in biochar, providing deeper insights into its thermoluminescent properties and their implications for dosimetry applications.

3.3. Structural analysis with XRD

The structural properties of biochar samples have been examined using XRD to determine the ordered and disordered carbon structures [30,31]. The structural changes of biochar samples exposed to gamma irradiation at doses ranging from 0 to 200 Gy has been analyzed by XRD. The XRD pattern of biochar shown in Fig. S4 has a broad hump in the 18.84°–28.15° region due to the plane index (002) [25,32]. Because of the aromatic and partially carbonized lamellae's parallel and azimuthal orientation, this (002) plane exists [33]. A sharp peak at 29.5° suggests the presence of minerals like calcium or potassium in biochar [34] with the space group of P63/mmc, $\alpha = 90°$, $\beta = 90°$, and $\gamma = 120°$. The lattice parameters are: a = 2.46, b = 2.46, and c = 6.71. All of these numbers are obtained from the matched database of ICDD. The volume of the unit cell, crystallite size, dislocation density, and micro-strain were also evaluated for the non-irradiated sample as well as for doses up to 200 Gy for gamma irradiated samples to observe the structural changes caused by radiation, as shown in Table S3. Fig. S5 depicts the XRD pattern for biochar irradiated at various doses. It can be confirmed from Table S3 that the Full width at half maxima (FWHM), peak intensity, peak area, crystallite size (L_c), dislocation density (δ), and lattice strain (ε) change with the radiation doses. The findings demonstrate that the size of the crystallites grows in proportion to the radiation exposure and that the dislocation density varies with the dose. The complex interactions between radiation energy and the microstructure of the material are responsible for this phenomenon. Higher radiation doses enhance atomic mobility, facilitating the coalescence of smaller crystallites into larger ones, a process known as grain growth. Conversely, the fluctuating dislocation density indicates a dynamic balance between defect generation and healing. Radiation may cause additional dislocations at lower doses, increasing the dislocation density. However, as the dose increases, the energy might encourage processes like recrystallization, which may heal underlying defects and lower dislocation density. These fluctuations suggest that the material undergoes structural rearrangements in response to varying radiation levels, reflecting the intricate interplay of processes governing its microstructural evolution [35–37]. The size of the crystallite has a substantial impact on the diffraction intensity. The FWHM increases with decreasing crystallite size [38]. Crystallite size and defect density are closely related, with an inverse relationship between them. As the crystallite size decreases, the defect density generally increases. This occurs because smaller crystallites have a higher proportion of atoms located near grain boundaries, where the crystal structure is more disordered compared to the interior. These grain boundaries introduce more defects, such as dislocations and vacancies, increasing the overall defect density. In contrast, larger crystallites have fewer grain boundaries relative to their volume, resulting in a more ordered structure and lower defect density. This inverse relationship is important because defects significantly influence the material's properties, including mechanical strength, thermal stability, and luminescence behavior. Table S3 shows that the variation in FWHM, area, crystallite size, dislocation density and microstrain, which confirms the creation of defects with the radiation dose.

3.4. TL measurement

3.4.1. Minimum Detectable Dose (MDD)

The minimum detectable dose (MDD) is the smallest amount of ionizing radiation that a detector is capable to detect. The MDD has been calculated using the formula $MDD = (B+2\sigma_B)F$; $F = 1/m$ from Ref. [39]. Where, B is the TL background signal derived from non-irradiated but only annealed samples, σ_B is the standard deviation for the mean background; F is the calibration factor = 1/m; (a reciprocal of the dose-response gradient, expressed in Gy/nC mg^{-1}), and m = slope from TL dose response. To ensure accuracy, the background signal was measured five times for each of the five TL dosimeters, and the results were documented for analysis. For biochar, the experimentally calculated MDD (based on the Harshaw TLD™ 3500 reader) for gamma irradiation has been estimated to be 1.3 Gy.

3.4.2. TL glow curve

A glow curve is the visual representation and the relationship between the temperature and thermoluminescence intensity. Prior to conducting the TL measurements reported in this study, the samples were assessed using various parameters of the TLD reader, with a particular focus on heating rates, as this significantly affects the glow curve and TL response. Test measurements were conducted at heating rates ranging from 2 °C/s to 15 °C/s on biochar samples subjected to 10 Gy of gamma irradiation at a maximum temperature of 300 °C. Fig. S6 shows the changes in glow curves at a constant gamma dose of 10 Gy. At lower heating rates the peak position is at a lower temperature and with the increasing heating rate the intensity was also increased and the peak temperature shifted to a higher temperature till 10 °C/s. These variations are attributed to the absence of a thermal quenching effect, as described by Ref. [40]. Moreover, the shifted peak position to a higher temperature positively contributes to the trap depth, kinetic parameters, stability and fading study [41]. Consistent with the findings of [8] using graphite material, who explored heating rates ranging from 2 to 15 °C/s, the observed glow curve patterns reinforce this conclusion. Notably, the glow curves in Fig. S6 indicate that a heating rate of 10 °C/s was optimally achieved and was chosen mainly due to the complete capture of the TL glow curve providing maximum TL yield with a peak maxima at higher temperature than other heating rates for biochar. Prior to conducting TL measurements, the acquisition temperature was optimized to 300 °C for biochar samples, similar to other carbonaceous materials [9,42]. Deeper traps may not fully depopulate at the acquisition temperature of 300 °C, meaning that as heating continues, trapped carriers are released at higher temperatures, causing the glow peak to shift. At lower acquisition temperatures, the system allows more time for charge carrier re-trapping, which can delay the release of trapped carriers and shift the glow peak to a higher temperature [18,43]. Higher acquisition temperatures provide sufficient thermal energy to release trapped carriers earlier in the heating cycle, even from deeper traps. The increased thermal energy accelerates trap activation, resulting in more traps being emptied compared to the lower temperatures and causing the glow peak to appear at a lower temperature. Additionally, thermal quenching at high temperatures may contribute to an earlier appearance of the glow peak. At higher acquisition temperatures, the rapid release of trapped charge carriers reduces the likelihood of re-trapping, which is opposite to the more carriers recombining at lower temperatures [18,43]. The thermoluminescence glow curve for the biochar sample, exposed within the dose range of 2 Gy–200 Gy of gamma irradiation has been shown in Fig. 1. From the glow curve of Fig. 1 it can be observed that a well-defined single glow curve is within the temperature of 50–300 °C and the maximum peak occurs well above 170 °C. It is also evident from Fig. 1 that when the irradiation dose rises, the intensity increases noticeably. Higher temperatures cause the electrons to be freed from deeper traps, which causes the TL peak to shift upward. Once more, there is a strong correlation between the number of trapped electrons and the radiation dose. The area under the peak shows a relationship between the quantity of radiation energy deposited and the number of electrons released from traps, where maxima indicates the maximum amount of electron release [44].

3.4.3. Dose response

In the present work, ^{60}Co gamma rays have been used to investigate

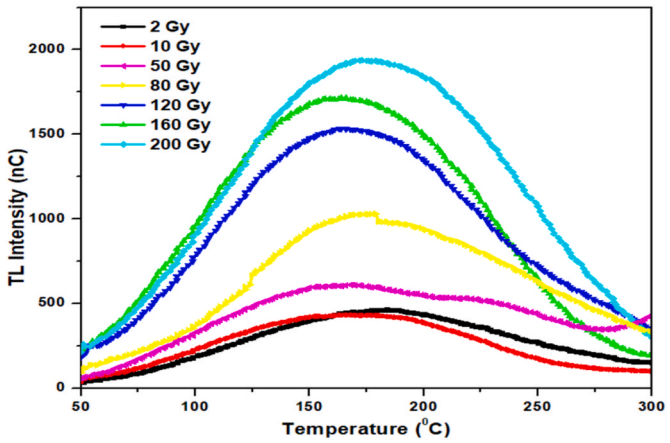

Fig. 1. TL glow curves for gamma irradiated biochar within the dose ranges from 2 Gy to 200 Gy.

the linearity of the dose-response over the range of 2–200 Gy. The dose-response shown in Fig. 2, illustrates the highly linear characteristic of the TL yield per unit mass with an R^2 coefficient of 0.99 for gamma-ray.

3.4.4. Sensitivity and linearity index

Fig. S7 illustrates the sensitivities, that are shown in terms of TL emission per unit dosage per unit sample mass. Each point represents the average readings of three samples. The highest sensitivity was found at the lowest given dosage over the whole dose range mediated by incident gamma-rays. The sensitivity decreases from 2 Gy to 50 Gy, then increases up to 80 Gy, and fluctuates thereafter. The fluctuations in TL intensity after 50 Gy may result from several factors, including radiation-induced defects and partial annealing, which can alter the availability of trapping sites. As the dose increases, trap saturation may occur, leading to non-linear TL responses due to recombination processes that do not produce light. Additionally, inhomogeneity in the sample, such as uneven distribution of carbon content or activators, can cause inconsistencies in the TL output. Self-attenuation effects at higher doses may further reduce the detected light intensity, contributing to the observed fluctuations [8,18,45]. The discrepancy in the sample's sensitivity at varying dosages could be caused by variations in the optical density, an uneven distribution of the carbon content throughout the sample, as well as variations in the sample's mass [46]. Given its excellent performance at low doses, biochar is well-suited for medical applications. In clinical settings, irradiation within the range of 1 Gy–10 Gy is commonly utilized for therapeutic interventions, including radiation therapy for conditions such as keloids, benign tumors, and palliative care aimed at alleviating symptoms in cancer patients [47]. Ensuring precise dose distribution during treatment planning is essential for optimizing therapeutic outcomes and maximizing the effectiveness of the intervention. The linearity index is plotted against various dosages in Fig. S8 to further illustrate the effects of dose linearity. The resultant mass and dosage-normalized TL intensity values were divided by the sensitivity at the lowest dose to determine the linearity index. A TL material is stated to have linearity, supralinearity, or sublinearity behavior for linearity index = 1, linearity index >1, or linearity index <1, respectively [48]. From Fig. S8, it can be observed that the biochar shows sublinearity after 2 Gy which might occur as a result of full occupancy at all available trapping or defect sites for electrons released during irradiation. This indicates that as the radiation dose increases, the response of the biochar also increases, but at a slower rate than would be expected in a perfectly linear relationship. Moreover, this condition may be attributed to the non-uniform spatial ionization density that occurs following X-ray and gamma-ray irradiation. This phenomenon has been effectively characterized by the Unified Interaction Model (UNM) [49]. As a result, rigorous calibration of the measurement device is essential to enhance the TL parameters and optimize the dosimetric performance of the material. However, this aspect falls outside the scope of the present investigation. It should be emphasized that the observed sublinear TL dose response does not constitute a significant limitation for the application of this material in TL dosimetry.

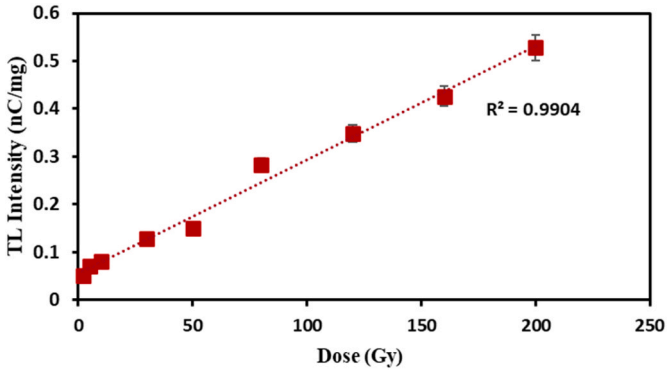

Fig. 2. The mass-normalized TL yield of biochar exposed 2–200 Gy of gamma radiation. The dotted lines provide the best fit to the measured data. Note that there is always less space between the error bars and the data points.

3.4.5. Repeatability

The perfect TL material should maintain its properties over cycles and be reusable multiple times without sensitivity or dose-response degradation. Five cycles of annealing, irradiation, and readout were used in the study to evaluate the repeatability of the biochar sample. The sample was subjected to a 400 °C annealing for an hour, followed by a 10 Gy exposure and the readout procedure in each cycle. Every data point represented the mean of three measurements taken from three aliquots. Five repetitions of these procedures were carried out in order to gather data on repeatability. As seen in Fig. S9, the examined sample demonstrated outstanding repeatability, with a standard deviation (SD) of less than 3 %. In medical dosimetry, a standard deviation (SD) of less than 5 % is deemed acceptable [2]. In the succeeding cycles, the examined sample's deviations from the first cycle were 1 %, 1.8 %, 2 % and 3 % respectively.

3.4.6. Fading

Fading is the loss of stored thermoluminescent signal, and it is mostly caused by the trap depth, storage temperature, and heat treatment used during annealing and readout [49]. The suggested TL materials must have a strong capacity to store the absorbed dosage for a prolonged amount of time, hence it is crucial to assess the fading qualities [50]. In this instance, the irradiated materials were stored in a darkened chamber following a fixed dosage of 10 Gy of gamma radiation and the TL signal degradation of biochar was observed during a period of 28 days. The mass normalized TL response for the biochar sample is depicted against storage duration (in days) in Fig. 3, with each point representing the mean of three observations made under the same circumstances. Fig. S10(a) represents the glow curve for each day. The TL signal loss was assessed by comparing the intensity with the measurement taken on the first day. The mass-normalized TL signal for various days showed losses of 1 %, 9 %, 14 %, and 19 % on the second, seventh, fourteenth, and twenty-eighth days, respectively, as shown in Fig. S10(b). The total estimated loss of TL response at 28 days post-exposure was 19 % in a dark room. Comparatively, previous studies have reported higher fading rates in other carbon-based materials. For instance Ref. [8], observed a 24 % TL signal loss in polymer pencil lead graphite (PPLG) over 21 days following gamma irradiation. Similarly [9], reported a 30 % TL signal loss in graphite sheets after 30 days for a 0.5 mm thick sample. In contrast, biochar demonstrated significantly lower fading, with the majority of TL loss occurring within the first 14 days post-irradiation. Additionally, the fading behavior of biochar is comparable to that of

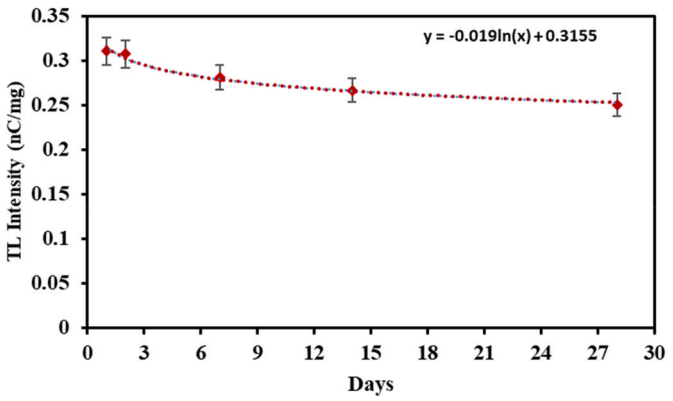

Fig. 3. Graph for fading of biochar sample exposed to a 10 Gy dose of radiation using ^{60}Co gamma rays. Note that the error bars are always smaller than the data points.

TLD-400 [51]. These findings suggest that biochar's fading characteristics are more stable than those of other carbonaceous materials studied, making it a promising candidate for dosimetry applications.

3.4.7. Optical bleaching

The residual TL yield of ^{60}Co gamma irradiated biochar at 10 Gy after exposure to fluorescent lab light throughout a 28-day storage period is shown in Fig. S11. Fig. S11 (a) demonstrates the mass normalized TL response over 28 days, while Fig. S11 (b) represents the TL glow curves for corresponding days. Light-induced fading of post-irradiated biochar was observed and found that the loss of signal was not too much. For the first 7 days, the loss of TL signal was only 9 %, and then it was found 17 % for over 28 days of post-irradiation. So, it can be observed that the loss of TL signal in light conditions doesn't differ greatly from dark conditions.

4. Conclusion

This work thoroughly explored the possibilities of utilizing biochar, an inexpensive and eco-friendly substance, in radiation dosimetry applications. The elemental, structural, and dosimetric studies were performed to assess the appropriateness of biochar as a radiation dosimeter. Findings indicate that the sample is suitable for use as TL dosimeters based on its excellent linearity of response, high sensitivity at lower doses, soft tissue equivalence effective atomic number, and good repeatability with a standard deviation of less than 3 %. It has been observed a low signal loss (~19 %) in the darkroom condition and ~17 % in the ambient conditions over 28 days after irradiation. The effects of gamma irradiation on the microstructures and defects in carbonaceous biochar were evaluated using Raman and XRD approaches. The alterations in the microstructures were verified throughout the investigated dose range of 2–200 Gy, which is indicative of the dosimetric characteristics of the biochar, hence the development of a cost-effective dosimeter for medical applications.

CRediT authorship contribution statement

Umme Muslima: Writing – original draft, Investigation, Formal analysis, Data curation. **Mayeen Uddin Khandaker:** Writing – review & editing, Supervision, Project administration, Methodology, Conceptualization. **S.N. Mat Nawi:** Writing – review & editing, Methodology, Investigation, Formal analysis, Data curation. **S.E. Lam:** Writing – review & editing, Investigation, Formal analysis, Data curation. **S.F. Abdul Sani:** Validation, Supervision, Methodology. **D.A. Bradley:** Writing – review & editing, Validation, Methodology. **Mustafa Mahmoud:** Writing – review & editing, Software, Resources, Project administration, Funding acquisition. **H.J. Woo:** Visualization, Validation, Software, Resources, Methodology.

Consent for publication

All authors of this work have agreed and are ready to sign the Transfer of Copyright which empowers the Publisher to protect the work against unauthorized use and to maintain the integrity of the work from a bibliographical and archival standpoint.

Availability of data and materials

All data are available in the manuscript.

Declaration of generative AI and AI-assisted technologies in the writing process

During the preparation of this work, the authors used some online services (such as Grammarly, Gemini, etc.) in order to improve language and readability. After using this tool/service, the authors reviewed and edited the content as needed and took full responsibility for the content of the publication.

Declaration of competing interest

The authors declare that they have no known competing financial interests or personal relationships that could have appeared to influence the work reported in this paper.

Acknowledgment

Ms. Umme Muslima expressed her deep appreciation to Sunway University for the PhD scholarship that enabled her to conduct this experimental study. The authors extend their appreciation to the Deanship of Research and Graduate Studies at King Khalid University for funding this work through Large Research Project under grant number RGP2/433/45.

Appendix A. Supplementary data

Supplementary data to this article can be found online at https://doi.org/10.1016/j.net.2024.103348.

References

[1] T. Kron, Applications of thermoluminescence dosimetry in medicine, Radiat. Protect. Dosim. 85 (1–4) (1999) 333–340.
[2] T. Rivera, Thermoluminescence in medical dosimetry, Appl. Radiat. Isot. 71 (2012) 30–34.
[3] A. Alanazi, et al., Carbon nanotubes buckypaper radiation studies for medical physics applications, Appl. Radiat. Isot. 117 (2016) 106–110.
[4] A. Alanazi, et al., Lower limits of detection in using carbon nanotubes as thermoluminescent dosimeters of beta radiation, Radiat. Phys. Chem. 140 (2017) 87–91.
[5] N. Bardi, et al., X-Ray irradiation-induced structural changes on single wall carbon nanotubes, Radiat. Phys. Chem. 140 (2017) 34–37.
[6] D. Bradley, et al., Raman spectroscopy and X-ray photo-spectroscopy analysis of graphite media irradiated at low doses, Appl. Radiat. Isot. 147 (2019) 105–112.
[7] L. Menichetti, et al., A micro-PET/CT approach using O-(2-[18F] fluoroethyl)-L-tyrosine in an experimental animal model of F98 glioma for BNCT, Appl. Radiat. Isot. 69 (12) (2011) 1717–1720.
[8] S.N.M. Nawi, et al., Polymer pencil lead graphite for in vivo radiation dosimetry, Diam. Relat. Mater. 106 (2020) 107860.
[9] S.E. Lam, et al., Carbon rich media for luminescence-based surface dosimetry and study of associated surface defects, Appl. Radiat. Isot. 199 (2023) 110920.
[10] J. Lehmann, S. Joseph, Biochar for Environmental Management: Science, Technology and Implementation, Taylor & Francis, 2024.
[11] S. McKeever, Thermoluminescence of Solids, Cambridge University Press, 1985.
[12] Y. Yan, et al., Synthesis of graphene oxide and graphene quantum dots from miscanthus via ultrasound-assisted mechano-chemical cracking method, Ultrason. Sonochem. 73 (2021) 105519.
[13] S.S. Sahoo, et al., Production and characterization of biochar produced from slow pyrolysis of pigeon pea stalk and bamboo, Cleaner Eng. Tech. 3 (2021) 100101.

[14] S.N. Mat Nawi, et al., Structural and dosimetric study of sub-kGy neutron-irradiated graphitic media, Radiat. Phys. Chem. 189 (2021) 109709.
[15] G. Duller, K. Penkman, A. Wintle, Assessing the potential for using biogenic calcites as dosemeters for luminescence dating, Radiat. Meas. 44 (5–6) (2009) 429–433.
[16] J. Garcia-Guinea, et al., Luminescence of strontianite (SrCO3) from strontian (Scotland, UK), Radiat. Meas. 44 (4) (2009) 338–343.
[17] K. Almugren, et al., Structural and defect changes in black carbon charcoal irradiated with gamma ray, Radiat. Phys. Chem. 200 (2022) 110331.
[18] S.W. McKeever, M. Moscovitch, P.D. Townsend, Thermoluminescence Dosimetry Materials: Properties and Uses, 1995.
[19] M.S. Seehra, A.S. Pavlovic, X-Ray diffraction, thermal expansion, electrical conductivity, and optical microscopy studies of coal-based graphites, Carbon 31 (4) (1993) 557–564.
[20] F.M. Khan, The Physics of Radiation Therapy, Lippincott, Williams & Wilkins, Baltimore, MD, 2010.
[21] B. Elman, et al., Structural characterization of ion-implanted graphite, Phys. Rev. B 25 (6) (1982) 4142.
[22] M. Kitajima, M. Okada, K. Aoki, Observation of shape change in the Raman spectrum of graphite exposed to deuterium glow, J. Nucl. Mater. 149 (2) (1987).
[23] K. Niwase, et al., On the amorphization of neutron-irradiated graphite, J. Nucl. Mater. 170 (1) (1990) 106–108.
[24] F. Cataldo, Spectroscopical characterization of carbonaceous matter prepared through the Glaser coupling reaction route, Carbon 37 (1) (1999) 161–163.
[25] Y. Huang, et al., Effects of metal catalysts on CO2 gasification reactivity of biomass char, Biotechnol. Adv. 27 (5) (2009) 568–572.
[26] F. Tuinstra, J.L. Koenig, Raman spectrum of graphite, J. Chem. Phys. 53 (3) (1970) 1126–1130.
[27] F. Rosenburg, et al., High-temperature Raman spectroscopy of nano-crystalline carbon in silicon oxycarbide, Materials 11 (1) (2018) 93.
[28] Y.-h. Shih, M.-s. Li, Adsorption of selected volatile organic vapors on multiwall carbon nanotubes, J. Hazard Mater. 154 (1–3) (2008) 21–28.
[29] Y. Yin, et al., Effect of char structure evolution during pyrolysis on combustion characteristics and kinetics of waste biomass, J. Energy Resour. Technol. 140 (7) (2018) 072203.
[30] V.S. Babu, M. Seehra, Modeling of disorder and X-ray diffraction in coal-based graphitic carbons, Carbon 34 (10) (1996) 1259–1265.
[31] G. Zheng, et al., Characterization of structural defects in nuclear graphite IG-110 and NBG-18, J. Nucl. Mater. 446 (1–3) (2014) 193–199.
[32] T. Chen, R. Liu, N.R. Scott, Characterization of energy carriers obtained from the pyrolysis of white ash, switchgrass and corn stover—biochar, syngas and bio-oil, Fuel Process. Technol. 142 (2016) 124–134.
[33] D. Mohan, et al., Biochar production and applications in soil fertility and carbon sequestration–a sustainable solution to crop-residue burning in India, RSC Adv. 8 (1) (2018) 508–520.
[34] B. Singh, M.D. Raven, 21 X-ray diffraction analysis of biochar, Biochar: Analytical Methods (2017) 245.
[35] J. Zhou, et al., The influence of oxygen vacancies on luminescence properties of Na 3 LuSi 3 O 9 : Ce 3+, J. Phys. Chem. C (2016) 120.
[36] F. Al-Mufadi, A. El-Taher, G. Gamal, Influence of γ-irradiation on the structural properties of indium monoselenide crystals, Eng. Technol. Appl. Sci. Res. 6 (6) (2016) 1264–1268.
[37] R. Krishna, et al., An understanding of lattice strain, defects and disorder in nuclear graphite, Carbon 124 (2017) 314–333.
[38] Z. Li, et al., X-ray diffraction patterns of graphite and turbostratic carbon, Carbon 45 (8) (2007) 1686–1695.
[39] C. Furetta, et al., Dosimetric characteristics of tissue equivalent thermoluminescent solid TL detectors based on lithium borate, Nucl. Instrum. Methods Phys. Res. Sect. A Accel. Spectrom. Detect. Assoc. Equip. 456 (3) (2001) 411–417.
[40] M. Kumar, et al., Effect of Heating Rate on TL Glow Curves–Theoretical and Experimental Studies, 2009.
[41] R.K. Tamrakar, et al., Effect of annealing temperature on thermoluminescence glow curve for UV and gamma ray induced ZrO2: Ti phosphor, Jj. Rad. Res. Appl. Sci. 8 (1) (2015) 1–10.
[42] S.M. Nawi, et al., The potential of polymer pencil-lead graphite for clinical electron beam dosimetry, Nucl. Instrum. Methods Phys. Res. Sect. A Accel. Spectrom. Detect. Assoc. Equip. 1010 (2021) 165478.
[43] R. Chen, Y. Kirsh, Analysis of Thermally Stimulated Processes, Pergamon, Oxford, 1981.
[44] M.U. Khandaker, et al., Thermoluminescent characterization and defect studies of graphite-rich media under high dose neutron exposure, Appl. Radiat. Isot. 196 (2023) 110771.
[45] A. Bos, High sensitivity thermoluminescence dosimetry, Nucl. Instrum. Methods Phys. Res. Sect. B Beam Interact. Mater. Atoms 184 (1–2) (2001) 3–28.
[46] M. Cholewa, B. Fischer, M. Heiß, Preparatory experiments for a single ion hit facility at GSI, Nucl. Instrum. Methods Phys. Res. Sect. B Beam Interact. Mater. Atoms 210 (2003) 296–301.
[47] H. Eyre, L. Blount, American cancer society, J. Oncology Practice 2 (2) (2006) 99.
[48] M. Begum, et al., Photonic crystal fibre as a potential medium for radiotherapy dosimetry, Appl. Radiat. Isot. 174 (2021) 109771.
[49] K. Almugren, et al., Thermoluminescence response of X-ray irradiated commercial chalk, Appl. Radiat. Isot. 151 (2019) 102–110.
[50] C. Furetta, Handbook of Thermoluminescence, World Scientific, 2010.
[51] H.A. Tajuddin, et al., Development of optical fibers for food irradiation dosimeter, Malays. J. Fundam. Appl. Sci 15 (2019) 109–111.